J Sol-Gel Sci Technol
DOI 10.1007/s10971-013-3018-5

Surface structure and reactivity study of phosphotungstic acid-nitrogenated ormosils

Elias P. Ferreira-Neto · Flavio L. S. de Carvalho · Sajjad Ullah · Vinicius C. Zoldan · André A. Pasa · Adriano Lopes de Souza · Liliane C. Battirola · Petra Rudolf · Sara Aldabe Bilmes · Ubirajara P. Rodrigues-Filho

Received: 1 February 2013 / Accepted: 15 March 2013

Abstract Supramolecular interactions between nitrogenated groups in hybrid ormosils bearing phosphotungstate nanocatalyst were used to tune the photocatalytical activity of these class-II hybrid materials obtained through sol–gel chemistry. Surface chemistry and morphology of the materials was studied by scanning electron microscopy, atomic force microscopy, X-ray photoelectron spectroscopy and water contact angle measurements. The photocatalytic efficiency of these hybrid films, measured by the degradation of crystal violet over-layer deposited on ormosils films, is higher for ormosils bearing neutral, more polar and less H-bonding nitrile groups than those bearing alkylamine/alkylammonium functionalities, despite the lower W/Si atomic ratio on the surface and lower tungsten percentage of the pure nitrile bearing ormosils. Such higher surface reactivity of the nitrile bearing ormosils is due to weaker interaction with the phosphotungstate and the lower activity of amine bearing ormosils is attributed to the competition among reversible photochromism and photocatalysis pathways in these materials.

Keywords Ormosil · Hybrid materials · Phosphotungstic acid · XPS · Photocatalysis · Supramolecular chemistry

1 Introduction

Hybrid materials are used as appropriate matrices in many applications because they offer the possibility to exploit the advantages of both organics and ceramics. Among the nanohybrid materials, class II ormosils (organically modified silicates) find wide-spread application in photonics [1], gaseous sensors [2], anti-corrosion coating [3] and proton-conducting hybrid membranes [4, 5]. Among the filmogenic hybrid materials, those bearing glycidyloxypropyl trimethoxysilane (Glymo) have attracted special attention [6] because of their superior mechanical and optical properties. These mechanical and optical properties can be improved further by addition of nitrogenated silanes, such as 3-aminoproyltrimethoxysilane (APTS). When incorporated into the Glymo-based ormosils, these nitrogenated silanes can act as curing agents by opening the oxyrane ring as well as catalyzing the alkoxy group hydrolysis in the Glymo molecule [7]. The cross-linking resulting from this kind of curing process results in good mechanical stability and better transparency.

Phosphotungstates (PWs), the representative polyoxometalates (POMs), are heteropolyanions with T_d symmetry displaying interesting photocatalytical and photochromic

Electronic supplementary material The online version of this article (doi:10.1007/s10971-013-3018-5) contains supplementary material, which is available to authorized users.

E. P. Ferreira-Neto · F. L. S. de Carvalho · S. Ullah · A. L. de Souza · L. C. Battirola · U. P. Rodrigues-Filho (✉)
Instituto de Química de São Carlos, Universidade de São Paulo, São Carlos 13560-970, Brazil
e-mail: biraprfilho@yahoo.fr; uprf@iqsc.usp.br

V. C. Zoldan · A. A. Pasa
Laboratório de Filmes Finos e Superfícies, Departamento de Física, Universidade Federal de Santa Catarina, Box 476, Florianópolis 88040-900, Brazil

L. C. Battirola · P. Rudolf
Zernike Institute for Advanced Materials, University of Groningen, Nijenborgh 4, 9747 AG Groningen, The Netherlands

S. A. Bilmes
Instituto de Química Física de los Materiales, Facultad Ciencias Exactas y Naturales, Universidad de Buenos Aires, Medio Ambiente y Energía—INQUIMAE, Ciudad Universitaria, Pab.2, C1428EHA Buenos Aires, Argentina

Published online: 22 March 2013

activity [8, 9]. PWs are usually incorporated by sol–gel method [10] into different matrices to prepare photocatalytic and photochromic devices [11–13]. Among hybrid materials, ormosils are the natural choice to develop devices based on POMs because they can be easily incorporated by bottom–up procedures. Furthermore, the properties of such polyoxometalates–ormosil hybrid materials can be tuned by exploiting polyoxometalates' intermolecular interactions with different organic functionalities [14, 15].

This study focuses on the surface characterization of the Glymo-nitrogenated silanes–phosphotungstate hybrid ormosils by SEM, AFM, XPS and water contact angle measurements. These new ormosils with Glymo form transparent photoactive films and monoliths, in contrast to the *N*-(3-(trimethoxysilyl)-propyl)-ethylenediamine/APTS (TSPEN/APTS) ormosils previously described [16]. The Photoactivity of the films, which is a surface-related phenomenon, was tested against crystal violet (CV), a water-soluble cationic triphenylmethane dye with wide-spread industrial applications, and which is known to cause acute oral toxicity carcinogenicity, DNA damage and mutagenicity [17, 18].

2 Experimental

2.1 Chemicals

Phosphotungstic acid hydrate (HPW), tetraethylorthosilicate (TEOS, 98 %), 3-aminopropyltriethoxysilane (APTS, 98 %), (3-glycidyloxypropyl)trimethoxysilane, (glymo, 98 %), and 4-(triethoxysilyl)butyronitrile (BuTs, 98 %) were purchased from Sigma-Aldrich (MA, USA) and used without further purification. Acetone, 99.5 %, was supplied by QHEMIS (SP, Brazil).

2.2 Film preparation

The sol formulations used in the film preparation are reported in Table 1. All solutions were prepared in Teflon or polypropylene reactors. The general procedure for all preparations was to add the silanes to the reactor with a micropipette followed by addition of 25 mL of acetone and then 25 mL of freshly prepared HPW solution in acetone under magnetic stirring. Finally 825 µL of deionized water was added and the mixture was left under magnetic stirring for 15 min before being used for film formation. Aluminosilicate glass slides (3 cm^2, Bioslide Technologies, Walnut, CA, USA) were treated following the adapted RCA procedure described by Donley et al. [19]. Films were prepared by dip-coating using an automatic disc elevator MA-765 Marconi (Piracicaba, SP, Brazil) and dried in ambient atmosphere (298 ± 2 K; relative humidity 60 ± 10 %). Ormosil powders were obtained by leaving the reaction mixture to dry under ambient conditions after covering the reactors with poly (vinyl chloride) film with small pores, as reported by De Oliveira Jr. et al. [16].

2.3 Characterization techniques

2.3.1 Elemental analysis

The carbon, hydrogen and nitrogen content of the ormosils was determined by an EA1110 CHNS-O Elemental Analyzer (Carlo Erba Instruments, Italy). The tungsten and silicon content was measured by X-ray fluorescence (XRF) analysis of the samples using an X Axios Advanced X-ray fluorimeter (PanAnalytical, The Netherlands). The samples were ground and pressed over a lithium borate powder using a hydraulic press to obtain double layered disks of ormosil/$Li_2B_4O_7$.

2.3.2 Atomic force microscopy

Contact mode AFM images were collected under nitrogen atmosphere with a PicoSPM (Molecular Imaging Corporation, USA) with a 6 µm tube scanner. The images were acquired in contact-mode using oxide sharpened 196 µm long SiN cantilevers with a force constant k = 0.58 N m^{-1} (model NP-S, Veeco, USA) and pyramidal tips with nominal curvature of 10 nm. The applied force was set between 3 and 10 nN. The scan line speed was optimized between 1 and 3 Hz over 512 × 512 pixels. Image treatment and analysis was done by Scanning Probe Imaging Processor (SPIP version 4.7, Image Metrology, Denmark). Definitions and formulas for root mean square roughness (R_{rms}) and surface area ratio (Sdr) are given in section S.1 of supplementary information.

2.3.3 Scanning electron microscopy

Ormosil films were examined by Zeiss-Leica/LEO 440 (LEO, UK) scanning electron microscope. Electron microprobe analysis was performed using an Energy Dispersive Spectrophotometer (Oxford Instruments, UK). All films were covered with an approximately 20 nm thick gold overlayer by sputtering using a MED 020 argon ion sputtering setup (Baltech, Germany).

2.3.4 X-ray photoelectron spectroscopy

X-ray photoelectron spectroscopy (XPS) data were collected using an SSX (Surface Science, USA) spectrometer equipped with a monochromatic Al Kα X-ray source (hν = 1486.6 eV); the photoelectron take-off angle was

Table 1 Sol-formulations used in the preparation of ormosil–HPW films

Ormosil code	[TEOS] mmol	[Glymo] mmol	[HPW] mmol	[APTS] mmol	[BuTS] mmol
A	9	6.8	0.75	2.25	–
B	9	6.8	0.75	–	1.50
AB	9	6.8	0.75	1.50	0.75

37°. An electron flood gun was used to compensate for sample charging and the base pressure during the measurement was 5×10^{-10} mbar. Samples were prepared by dip-coating on aluminosilicate glass. Binding energies were referenced to the Si2p core level at 103.2 eV. Deconvolution of spectra included Shirley baseline fitting using the least-squares curve fitting program Winspec developed at the Facultés Universitaires Notre Dame de la Paix, Namur, Belgium; the profile of the peaks was taken as a mixture of Gaussian and Lorentzian functions. Quantitative analysis was performed taking into account the sensitivity factors for each element, specific to the spectrometer used.

2.3.5 Contact angle measurements

The water static contact angles were determined by the sessile drop method with a home-made goniometer equipped with a CCD camera coupled to an optical microscope (MM Optics, Brazil). A 1.2 μL droplet of Milli-Q water was deposited on the films supported on aluminosilicate glass placed in a home-made acrylic chamber at (298 ± 1) K and 65 % of air relative humidity. Contact angle measurements were made after 30 s.

2.4 Photocatalytical tests

The photoactivity of the hybrid ormosils films supported on glass substrates was tested by measurement of the area under the absorbance peak of the CV over-layer deposited on the ormosils films before and after 10 min of UV-irradiation with a 16S SolarLight Xe arc lamp of 150 W(Solar Light Co., USA). The lamp-to-film distance was 8 cm and the UVA and UVB dose was 59.8 and 4.60 J cm^{-2}, respectively, for 10 min of irradiation. The Xe arc lamp operate with an automatic shutter and internal near infrared filter in conjunction with a PMA2100 radiometer equipped with PMA 2110 UVA and PMA 2106 UVB detectors. A control experiment was also run by directly irradiating the CV layer on a bare glass plate (without ormosil film) to estimate the direct photolysis. All measurements were taken in a transmission mode.

3 Results and discussion

3.1 Surface characterization

3.1.1 Scanning electron microscopy

Scanning electron microscopy micrographs of the samples are very similar and show quite smooth surfaces with few protrusions. Electron microprobe analysis showed a homogeneous distribution of Si and W (Fig. 1). Such uniform dispersion of phosphotungstate in the ormosil matrix is due to the complete solubilization of the HPW in the silane–acetone mixture during the synthesis step. Therefore, once added to the silane solution, HPW interacts as individual molecule randomly distributed in the solution. It is important to remark that all synthesis with APTS form dispersions instead of real solutions which indicates the formation of an ion pair upon mixing HPW and APTS, as explained later. Such strong interaction must affect the surface morphology of the APTS-bearing ormosils. Therefore, AFM, XPS and water static contact angle measurements were performed to address this aspect.

3.1.2 Atomic force microscopy

The 2 × 2 μm^2 AFM surface topography images along with the corresponding line-scanes of ormosil-A and ormosil-B are shown in Figs. 2 and 3 respectively. The samples exhibit quite similar value of Root mean square roughness (R_{rms}) which is (0.83 ± 0.20) nm for ormosil-A and (1.30 ± 0.13) nm for ormosils-B; sample AB display values in-between. These results agree with data reported previously for other sol–gel films [20].

All ormosils with BuTS display a slightly higher roughness as can be noted from a comparison of the line scans in Figs. 2 and 3 as well as from the higher surface area ratio of ormosils-B. The surface area ratios were found to be (0.12 ± 0.10) % and (0.23 ± 0.06) % for ormosil-A and ormosil-B, respectively. The R_{rms} values and surface area ratio deduced from the 6.5 × 6.5 μm^2 images (not shown) are (6.4 ± 0.8) nm and (0.079 ± 0.020) % for ormosil-A and (5.60 ± 1.1) nm and (0.14 ± 0.09) % for ormosil-B. These values allow us to classify the surfaces as flat. The slightly higher roughness of ormosils-A at larger scales is probably related to the formation of a colloidal dispersion instead of a solution during synthesis.

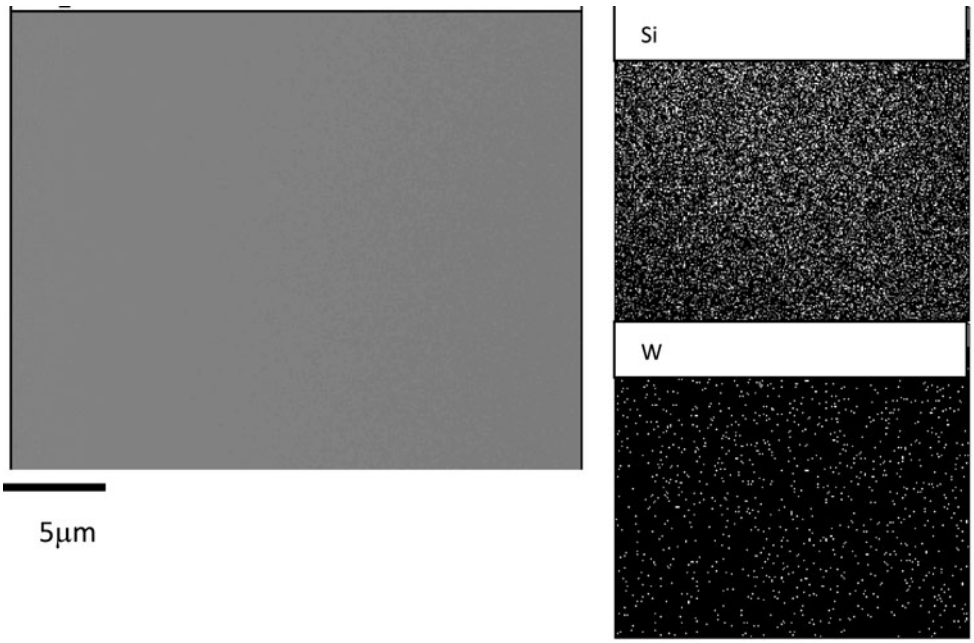

Fig. 1 SEM image of the sample A with Si and W X-ray emission mapping

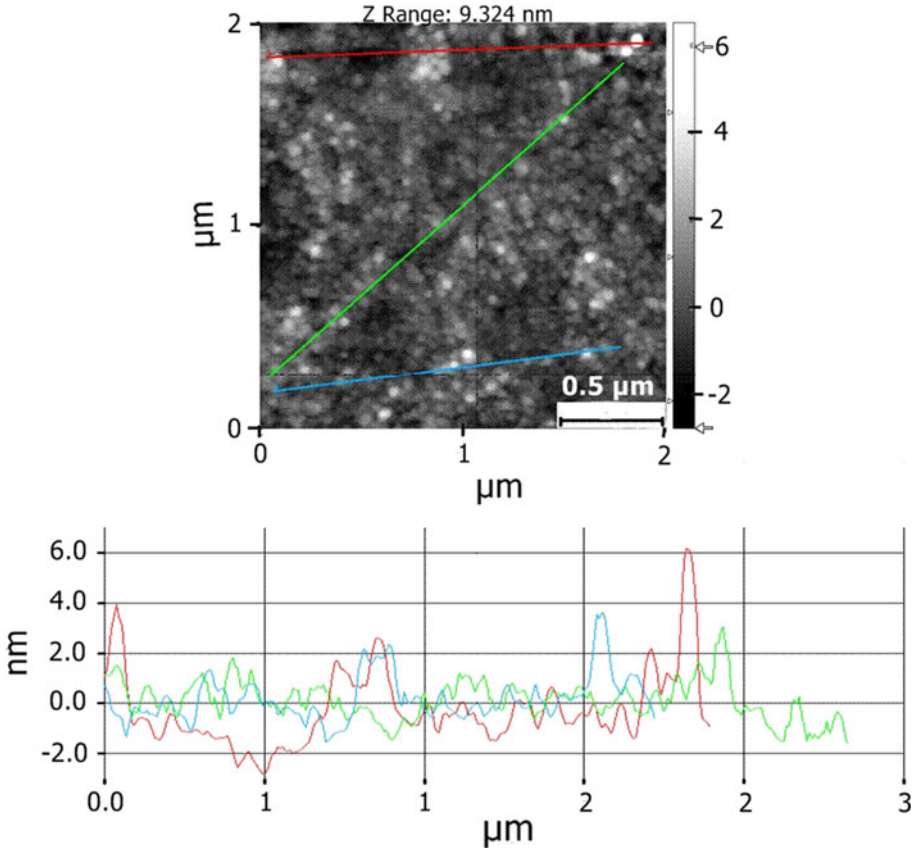

Fig. 2 Contact mode atomic force micrograph (2 × 2 µm^2) of ormosil-A: topographic image (*above*) and line scans (*below*) along the three tracks marked in the *image above*

3.1.3 X-ray photoelectron spectroscopy

The presence of HPW on the surface of the films was confirmed by XPS measurements. Figure 4a presents the survey spectrum for ormosil-A, which is representative for all ormosils. The spectrum shows the core level lines for Si, C, O, N and W.

The bulk elemental analysis of various elements in the films was carried out for a better understanding and comparison with the surface elemental composition of the films

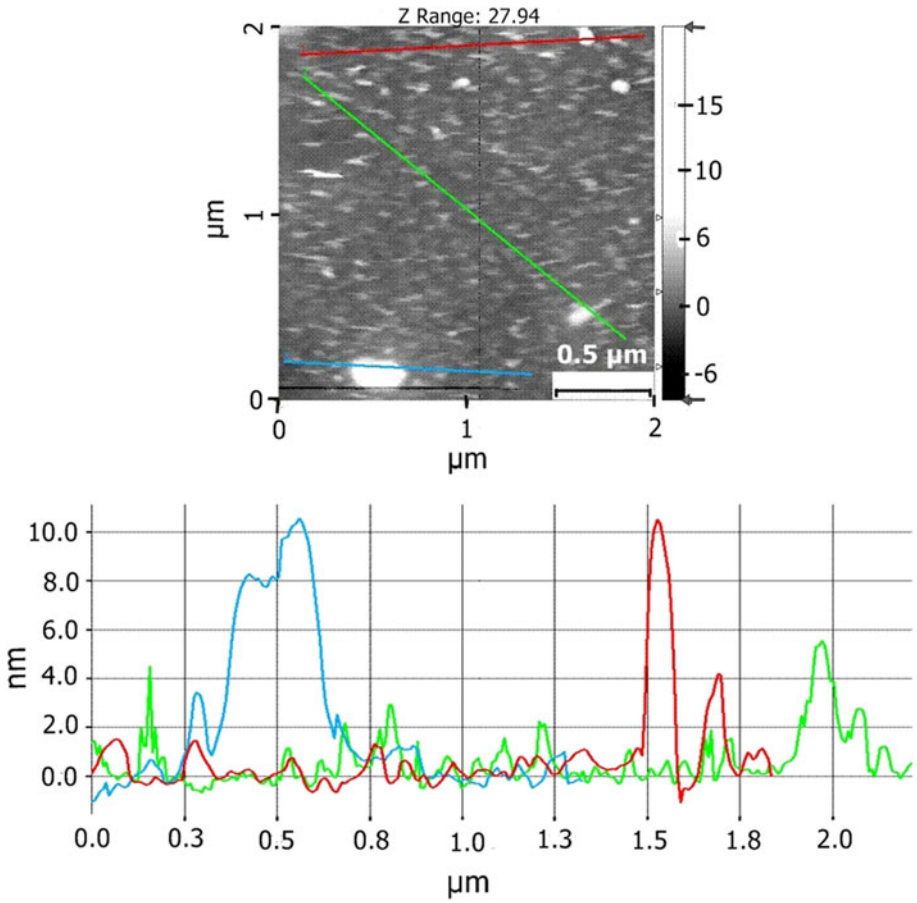

Fig. 3 Contact mode atomic force micrograph (2×2 µm^2) of ormosils-B: topographic image (*above*) and line scans (*below*) along the three tracks marked in the *image above*

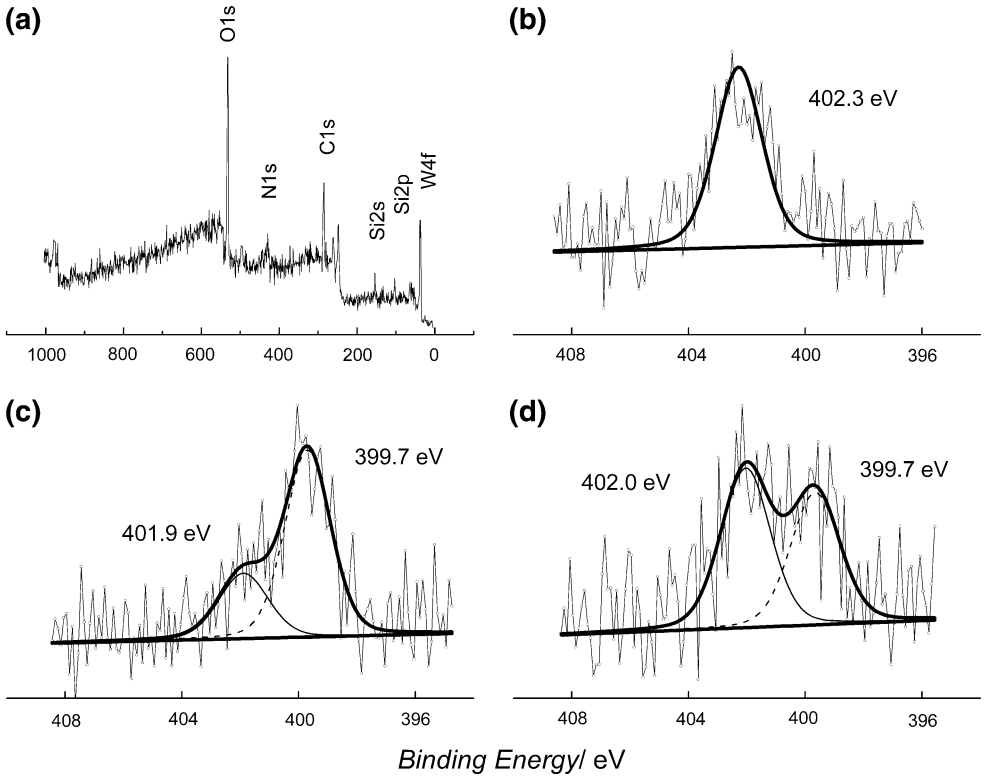

Fig. 4 Overview X-ray photoemission spectrum (**a**) and detail of the N1 *s* core level region for ormosil-A (**b**), ormosil-B (**c**), ormosil-AB (**d**)

obtained with XPS. The C, H, N and W content of the ormosils coded as A, B and AB as well the atomic ratios determined by XPS and elemental analysis are listed in Table 2.

The N/C ratios obtained by XPS are similar for all samples as expected since the nitrogenated species used in the ormosil synthesis have propyl and ethyl chains, and the bulk nitrogen atomic percentages, N %, are about the same. More significant is the N/Si ratio, since the N 1 *s* signal is related only to nitrogenated silanes, while the Si 2*p* intensity accounts for all alkoxysilicon species used in the synthesis. It can be noted from a comparison of the N/Si atomic ratios at the surface (XPS) and bulk (elemental analysis) that nitrogenated species tend to occupy the surface. However, this tendency is less pronounced in ormosil-A compared to ormosil-B and ormosil-AB. Ormosil-B, obtained by using the BuTS silane instead of the APTS silane, displays the highest N/Si ratio in agreement with the highest bulk nitrogen percentage of the ormosils (Table 2). Similarly, ormosil-AB displays the second highest N/Si atomic ratio as is its bulk nitrogen percentage. Ormosil-A, which is richer in the $-NH_2$ groups, showed lower N/Si atomic ratios. Therefore, compared to nitriles-bearing silanes, the nitrogenated silanes with $-NH_2$ groups are preferentially buried in the bulk of the material.

These nitrogenated silanes with $-NH_2$ groups probably have faster hydrolysis-condensation kinetics, forming particles richer in amino/ammonium groups. We suggest that this is due to $-NH_2$ group of APTS, which acts as catalyst in alkoxy group hydrolysis by H-bonding to oxygen of the Si–O-R groups, thus inducing a higher susceptibility of Si for hydrolyses by nucleophilic species, resulting in a faster hydrolysis rate [21, 22]. The N/W atomic ratio is higher for ormosil-B, reflecting the higher surface concentration of N and lower concentration of W for this ormosil (Table 2). Generally, higher content of APTS results in a lower N/W ratio at the surface, pointing to $-NH_3^+$ formation during the synthesis described by the following reactions:

$$H_3PW_{12}O_{40} \cdot nH_2O + \text{Solvent} \rightarrow 3[(H_5O_2)]^{(+)}_{(\text{solvated})} + [PW_{12}O_{40}]^{3-}_{(\text{solvated})} \quad (1)$$

$$[(H_5O_2)]^{+}_{(\text{solvated})} + H_2N-(CH_2)_3-Si-\text{Ormosil} \rightarrow \left[H_3N^+-(CH_2)_3-Si-\text{Ormosil}\right] \times 2H_2O + \text{Solvent} \quad (2)$$

The NH_3^+ formation is supported by the analysis of the binding energies of the N1 *s* XPS spectra in Fig. 4. The profile of the N1 *s* peak for the ormosils-A (Fig. 4b) was fitted as a single nitrogenated species on the surface. The asymmetric N1 *s* lines of the other ormosils were fitted with two singlet pseudo-Voigt functions with similar Gaussian/Lorentzian ratio as the ormosil-A N1 *s* line. The symmetric N1 *s* component of ormosil-A appears at a binding energy of 402.3 eV, while the high binding energy N1 *s* components of ormosils AB occur at 402 eV which we tentatively assign to $-NH_3^+$ groups formed by the reaction of solvated protons and $-NH_2$ groups. It is remarkable that the N1 *s* spectrum of ormosil-A displays only one component, thus indicating full conversion of $-NH_2$ to $-NH_3^+$ on the surface.

The component at a binding energy of 401.9 eV in the asymmetric N1 *s* line of ormosil-B can be tentatively

Table 2 Elemental content in percent (w/w) and atomic ratios of the elements in ormosils powders as determined by bulk elemental analysis (C, H, N) and XRF (W, Si) and atomic ratios of the elements in the ormosil films as deduced from the XPS intensities

Analysis	Ormosil samples		
Chemical analysis (w/w %)	A	B	AB
%C	17.0 ± 0.6	14.0 ± 4.5	13.0 ± 3.8
%H	3.7 ± 0.13	3.0 ± 0.56	2.9 ± 0.61
%N	1.1 ± 0.12	1.8 ± 0.20	1.5 ± 0.39
%W	42 ± 3.00	34 ± 3.50	49 ± 3.80
%Si	10.0 ± 0.31	12.0 ± 0.35	7.20 ± 0.42
Atomic ratios by elemental analysis			
N/C	0.05	0.11	0.10
N/Si	0.22	0.30	0.41
N/W	0.34	0.69	0.40
W/C	0.15	0.15	0.24
W/Si	0.63	0.43	1.03
Atomic ratios by XPS			
N/C	0.41	0.49	0.55
N/Si	0.88	1.37	1.04
N/W	0.57	1.57	0.63
W/C	0.72	0.31	0.87
W/Si	1.54	0.87	1.66

assigned to the formation of the $-CH_2=NH_2^+$ species on the surface [23] or to protonated nitrile groups, [ormosil–Si–$(CH_2)_3$–C≡N–H]$^+$(solvated) [24]. Protonation of the nitrile group would affect the binding energy similarly as the coordination of pure σ-bonding Lewis acids, such as for instance BF_3. Coordination of BF_3 to nitrile groups forming a Lewis adduct with B–N bonding results in a 2.3–2.8 eV shift towards higher binding energy [25].

Figure S2 shows the W4*f* doublet and 5*p* core level region of the XP-spectrum of ormosil-A, representative for all samples. The occurrence of the W4*f* $_{7/2}$ and W4$f_{5/2}$ doublet and W5*p* peaks at such high binding energy confirms the presence of HPW on the surface.

The W4$f_{7/2}$ peak for the ormosils A, B and AB was found to occur at binding energies of 36.2, 35.8 and 35.1 eV, respectively. For hydrated HPW polycrystalline samples the W4$f_{7/2}$ peak is situated at 36.0 eV [26]. It can be observed that higher N % (Table 2) and lower [APTS]/[BuTS] ratios result in lower W4$f_{7/2}$ binding energies. For ormosils-AB, ormosil with mixed nitrogenated silanes, only one W4*f* doublet is observed, indicating that, at least on the surface, APTS and BuTS silanes are not forming different domains. Hence the formation of mixed domains with $-NH_3^+$ and –CN groups is most likely. These mixed domains generate and average the environmental potential, resulting in different chemical shifts observed for the W4$f_{7/2}$ peak of the different ormosils. The C1 *s* and Si2*p* lines are related to the silica–glymo network of the hybrid material. Table 2 shows that the W/C and W/Si atomic ratios are lower for ormosil-B in agreement with the lower tungsten atomic percentage, W %, in the bulk.

3.1.4 Water contact angle measurement

Static water contact angle measurements gave angles around (60.0 ± 1.8)°, testifying a more hydrophobic character of the ormosils as compared to the clean aluminosilicate glass used as support or to a silica xerogel film (obtained by acid catalysis of the TEOS hydrolysis) on aluminosilicate glass, which yielded a contact angle of (24.0 ± 3.1)°. The ormosil film obtained by the HPW catalyzed co-hydrolysis of APTS and TEOS (without Glymo) shows a static water contact angle of (47.0 ± 1.7)°. Hence, the use of glymo results in a more hydrophobic material. One can deduce that glymo and other oxygenated groups less polar than the $-NH_2$ and $-NH_3^+$ groups of APTS preferentially occupy the surface, probably due to the lower polarity of Glymo as compared to BuTS and APTS.

Summarizing the results, water static contact angle, AFM and EDX have not been able to see the differences among the samples, despite XPS shows difference in the N/W and N/Si surface atomic ratios among the APTS ormosils (A and AB) and the BuTS ormosil (B). It turns out that the surface energy of these materials is dominated by glymo-derived functionalities, phosphotungstate and silicate.

Probably, the relative nitrogenated silane bulk segregation for A and AB ormosils is related to the formation of nanodomains rich in nitrogenated silanes in a similar way as observed by Atanacio et al. [27] for other hybrid ormosils.

3.2 Surface reactivity (photocatalytic activity)

The prepared hybrid ormosils showed good photoactivity as measured by the degradation of an over-layer of CV deposited on the surface of hybrid ormosil films. Figure 5 shows the electronic absorption spectra of CV over-layer on the surface of ormosil-AB film. The decrease in absorbance of CV peaks after 10 min of irradiation with UV shows the degradation of CV by the hybrid ormosil film. A similar change is observed in presence of ormosils-A and ormosils-B but to different degree. Figure 6 gives a comparison of the photoactivity of the three types of hybrid films. The direct photolysis of CV by the UV in absence of photoactive hybrid films (only CV layer on bare glass) is also shown for comparison.

It can be noted from Fig. 6 that all the three type of ormosil films depict good photoactivity, to variable extents, towards the degradation of CV as compared to direct photolysis. The lowest photodegradation of CV (about 20 %) is observed in case of ormosils-A, while the photodegradation in case of other two ormosils (B and AB), both of which bear nitrile groups, is twice that of A. Apparently, higher concentration of APTS in the sol

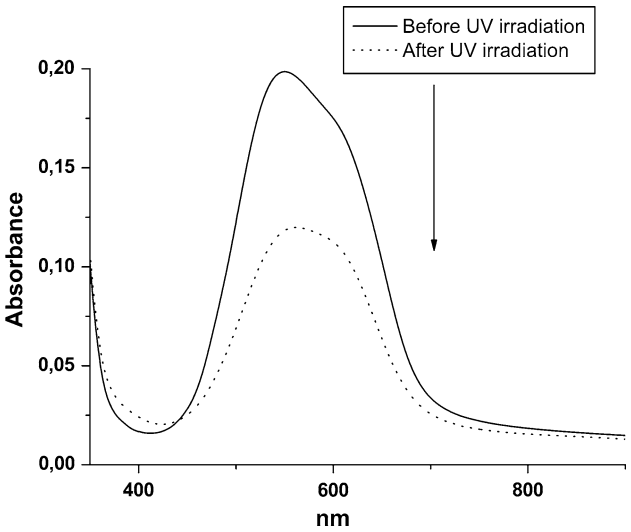

Fig. 5 Electronic absorption spectra of the CV over-layer deposited on surface of ormosils-AB film formed on glass plate before (*full line*) and after UV irradiation (*dotted line*) for 10 min

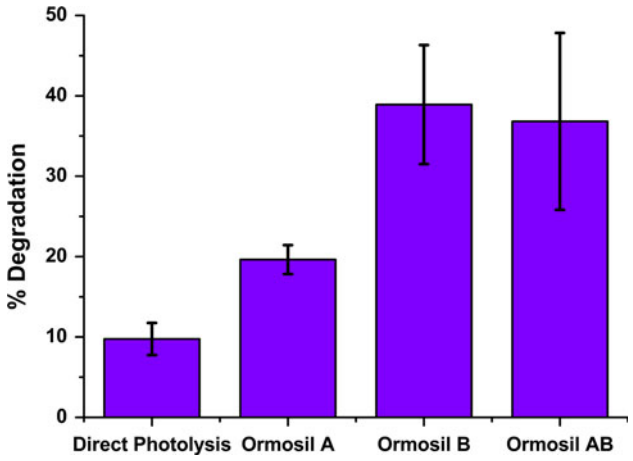

Fig. 6 A comparison of Photodegradation of CV over-layer by the three type of ormosil films and in the absence of any photoactive film (direct photolysis by UV radiation) after 10 min of irradiation with UV-light from a Xe arc lamp

composition (ormosil-A) diminishes the photocatalysis by phosphotungstate heteropolyanions. As discussed previously, the surface of the all these films is quite similar, so the different photocatalytic behavior is not explained by differences in surface characteristics such as R_{rms}, area ratio or photocatalyst distribution. For example, the percentage of dye degradation promoted by ormosil-B is remarkable, though this material presents the lowest W/Si and W/C ratios (lowest concentration of photocatalyst on surface). This difference can be readily understood by considering the electronic properties of the phosphotungstate and the interactions of this specie with different functional groups in each material. Photocatalysis promoted by phosphotungstates is based on the generation of holes in the HOMO by photo-excitation of O → W ligand to metal charge transfer (LMCT) transition [8, 9]. It is commonly accepted that the excited state of polyoxometalates can form charge transfer complexes with ammonium groups, and this interaction stabilizes the generated blue species (heteropolyblues) by proton donation, stabilizing the electron promoted to the LUMO, and a simultaneous interaction of the hole in HOMO with non-bonding electrons on nitrogen atom of ammonium group. This kind of interaction was first proposed by Yamase [9] in his studies of alkylammonium polyoxometalates, and has been exploited for the enhancement of photochromic properties of POM-based materials [16]. While stabilization of the photo-reduced phosphotungstate enhances the photochromic response, it can diminish the photocatalysis by reducing the photo-generated holes or reactive species like hydroxyl radicals which are responsible for photodegradation of organic compounds. It is thus inferred that the presence of excess amine functionalities in ormosil-A is responsible for its lower photocatalytic activity. On the other hand, nitrile groups present in ormosil B and AB seem to have no such deactivating interaction with the excited phosphotungstate, and thus B and AB show higher photoactivity compared to A. The ongoing research in our group (results not published yet) also indicated that ormosil B has lower photochromic response compared to ormosil A and AB, thus further confirming our conclusion.

4 Conclusion

The solid-state photocatalytical activity toward crystal violet films deposited on hybrid inorganic–organic ormosils doped with phosphotungstic acid can be tuned by the ratio of amine and nitrile organosilanes used in the ormosil synthesis. Higher photoactivity is achieved by using BuTS nitrile bearing silanes exclusively or mixed with the aminosilane, APTS. XPS revealed a surface depleted in nitrogen in the ormosil with aminosilane APTS which can explain the contact angle, since nitrogen depletion results on surface layer richer on silicate groups or even silica nanodomains. Thus, fine tuning of photochemical activity of these materials can be obtained by controlling phosphotungstate-matrix supramolecular interaction by varying the amine/nitrile ratio in the ormosils.

5 Supporting information

Data for root mean-square roughness and surface area ratio equations is available in the Supplementary Section.

Acknowledgments Part of this work was performed within the exchange program of the Instituto de Química de São Carlos, Universidade de São Paulo and the Faculty of Mathematics and Natural Sciences of the University of Groningen. The authors acknowledge the Panalytical Brazil for XRF measurements. We acknowledge the funding by the São Paulo Research Foundation (FAPESP) Grant # 2011/08120-0 and the National Council for Scientific and Technological Development (CNPq) Grant # 479748/2008-0. F.L.S. de Carvalho and E. P. Ferreira Neto thank the Coordenação de Aperfeiçoamento de Pessoal de Nível Superior (CAPES) for Brazilian studentships; L.C. Battirola thanks CAPES Grant # 5321-09-3 for the international exchange fellowship Brazil/The Netherlands. S. Ullah thanks the Third World Academy of Science (TWAS) and the National Council for Scientific and Technological Development (CNPq, Brazil) for Ph.D fellowship.

References

1. Pénard AL, Gacoin T, Boilot JP (2007) Acc Chem Res 40:895–902
2. Orel B, Groselj N, Krasovec UO, Jese R, Georg A (2002) J Sol-Gel Sci Technol 24:5–22
3. Surca Vuk A, Fir M, Jese R, Vilcnik A, Orel B (2008) Progr Org Coat 63:123–132

4. Mosa J, Durán A, Aparicio M (2010) J Membr Sci 361:135–142
5. Sanchez C, Julian B, Belleville P, Popall M (2005) J Mater Chem 15:3559–3592
6. Etienne P, Denape J, Paris JY, Phalippou J, Sempere R (1996) J Sol-Gel Sci Technol 6:287–297
7. Kim DH, Moon JH, Lee DW, Shul YG (2003) J Sol-Gel Sci Technol 26:403–406
8. Hiskia A, Mylonas A, Papaconstantinou E (2001) Chem Soc Rev 30:62–69
9. Yamase T (1998) Chem Rev 98:307–326
10. Sakka S (2005) Handbook of sol-gel science and technology: processing, characterization and applications. Vol. 1–3 Springer, New York
11. Judeinstein P, Schmidt H (1994) J Sol-Gel Sci Technol 3:189–197
12. Kukovecz Á, Balogi Zs, Kónya Z, Toba M, Lentz P, Niwa SI, Mizukami S, Molnár Á, Nagy JB, Kiricsi I (2002) App Catal A: General 228:83–94
13. Souza AL, Marques LA, Eberlin MN, Nascente PAP Jr, Leite FL, Rodrigues-Filho UP (2012) Thin Solid Films 520:3574–3580
14. Zhang XE, Wu WJ, Wang JF, Liu CL, Qian SW (2008) J Mater Res 23:18–26
15. Huang Y, Pan QY, Dong XW, Cheng ZX (2006) Mat Chem Phys 97:431–436
16. De Oliveira M Jr, de Souza AL, Schneider J, Rodrigues-Filho UP (2011) Chem Mater 23:953–963
17. Subnis RW (2008) Hand-book of acid-base indicators. CRC Press, Boca Raton, pp 108–110
18. Subnis RW (2010) Handbook of biological dyes and stains: synthesis and industrial applications, John Wiley and Sons, New Jersy, pp–116
19. Donley C, Dunphy D, Paine D, Carter C, Nebesny K, Lee P, Alloway D, Armstrong NR (2002) Langmuir 18:450–457
20. Nellis BA, Satcher JH, Risbud SH (2011) Acta Biomater 7: 380–386
21. Kobayashi J, Kawaguchi K, Kawashima T (2004) J Am Chem Soc 126:16318–16319
22. Eaton P, Holmes P, Yarwood J (2001) J Appl Polym Sci 82: 2016–2026
23. Williams JM, Peterson SW, Brown GM (1968) Inorg Chem 7:2577–2582
24. Drago RS, Dias JA, Maier TO (1997) J Am Chem Soc 119: 7702–7710
25. NIST X-ray photoelectron spectroscopy database, Version 3.5 (National Institute of Standards and Technology, Gaithersburg, 2003); http://srdata.nist.gov/xps/
26. Oliveira FC, Schneider JF, Siervo A, Landers R, Plepis AMG, Pireaux JJ, Rodrigues-Filho UP (2002) Surf Interface Anal 34:580–582
27. Atanacio AJ, Latella BA, Barbe CJ, Swain MV (2005) Surf Coat Technol 192:354–364